THEORETICAL STUDY OF A NANOFLUID SOLAR COLLECTOR ASSISTED- HYBRID DESALINATION SYSTEM FOR SMALL COMMUNITIES NEEDS

Emad M. S. El-Said[1], A. E. Kabeel[2]

1 Industrial Engineering Department, Faculty of Engineering, Fayoum University, Fayoum, Egypt. *E-mail:* emad_mech@hotmail.com
2 Mechanical Power Engineering Department, Faculty of Engineerin, Tanta University, Tanta, Egypt . *E-mail:* kabeel6@hotmail.com

ABSTRACT

This paper introduces an innovative hybrid desalination system coupled with nano-fluid solar heater for small scale needs. The hybrid desalination system consisting of a two stages of humidification dehumidification unit and single stage flashing evaporation unit (MEH-SSF) configured by a (Al_2O_3/H_2O) nano-fluid solar water heater under the climatologically conditions of Tanta city, Egypt. A theoretical study has been carried out according to actual thermal environment. This system was designed and modeled using finite deference scheme in steady state conditions. The governing equations of the model are solved by theoretical code using MATLAB®. A seven main parameters that have influence on the system productivity is studied; feed water mass flow rate of SSF unit, feed water mass flow rate of HDH units, cooling water mass flow rate of SSF unit, cooling water mass flow rate of HDH units, air mass flow rate, inlet cooling water temperature and nano-particle volume fraction. The economic analysis was to show both the economic benefits and the feasibility measurement. The total cost of ownership (TCO) concept was adopted in the analysis. The results show that, the studied hybrid desalination system gives a significant operational compatibility between the air humidification dehumidification method and flash evaporation desalination with daily water production up to 112.5 kg/day. The efficiency of the system is measured by the gained output ratio (GOR) with day time. The gained output ratio (GOR) of the system reaches 7.5. The effect of the water and the air solar heaters collecting areas on the system productivity is measured. The solar water heater efficiency is affected by the nano-particle volume fraction by increasing the fresh water production and decreasing cost. Solar water heater efficiency is about 49.4%. Based on the cost of energy in Egypt, the estimated cost of the generated potable water was 6.43 US$/m^3. The current study showed that the plant lifetime is considered significant factors for reducing the water production cost.

1 INTRODUCTION

The worldwide demand for fresh water is escalating due to the population growth and ever-increasing industrialization of our society. The worldwide effect of such demand rises, combined with the substantial decline of natural resources is Currently affecting 25% of the world's population across 50 countries where the water shortage has already reached a critical stage. The

shortage of fresh water affects poor and rich countries alike primarily because the arid and semi-arid regions spread across the globe not only in the third world countries but in rich countries, such as USA, UK and Australia. The rest exists in lakes, rivers and underground reservoirs. Natural resources cannot satisfy the growing demand for low-salinity water with industrial development, together with the increasing worldwide demand for supplies of safe drinking water. This has forced mankind to search for other sources of water. In addition, the rapid reduction of subterranean aquifers and the increasing salinity of these nonrenewable sources will continue to exacerbate the international water shortage problems in many areas of the world. Desalination has already become an acceptable solution for shortages in conventional water resources. This is now acknowledged by reputable institutions such as the World Bank. Seawater desalination is being applied at 58% of installed capacity worldwide, followed by brackish water desalination accounting for 23% of installed capacity. Due to the limited fossil fuel resources, it is expected that their price continues to rise dramatically in the future. On the other hand climate change obliges humanity to react accordingly. Renewable energy is the favorable alternative to fossil fuels. Solar energy can be used for saline water desalination either by producing the thermal energy required to drive the phase-change processes by using direct solar collection systems. Garg et al. [1] presented an experimental design and computer simulation of multi effect humidification–dehumidification solar desalination and the developed model which is useful in the estimation of the distillation plant output and optimized various components of the system like, solar water heater, humidification chamber, and condensation chamber. Dai et al. [2] conducted experimentally a solar desalination unit with humidification and dehumidification. The performance of the system was strongly dependent on the temperature of inlet salt water to the humidifier, the mass flow rate of salt water, and the mass flow rate of the process air. The optimum rotation speed for the fan corresponding to an optimum mass flow rate of air with respect to both thermal efficiency and water production. The unit worked perfectly and the thermal efficiency was above 80%. Nafey et al. [3,4] investigated numerically and experimentally a humidification dehumidification desalination process using solar energy under different environmental and operating conditions. The comparison between theoretical and experimental results illustrated that the mathematical model are in good agreement with the experimental results. The productivity of the unit is strongly influenced by the air flow rate, cooling water flow rate and total solar energy incident through the day. The obtained results indicate that the solar water collector area strongly affects the system productivity, more so than the solar air collector area. El-Shazly et al. [5] took another way with humidification–dehumidification desalination method to enhance mass and heat transfer rates, and improve both process productivity and product quality by using pulsating liquid flow. An experimental investigation was performed in humidification–dehumidification desalination unit consists of the main components (humidifier, dehumidifier, and solar water heater). The results showed that the unit productivity has been increased by increasing the off time i.e. decreasing the frequency of pulsed water flow up to certain levels, a frequency of 20/60 on/off time was found to have the highest productivity of the unit. Increasing the amplitude of water pulsation (water flow per pulse) was found to increase the unit productivity as well. Nafey et al. [6] investigated theoretically and experimentally a small unit for water desalination by solar energy and a flash evaporation process. The system consists of a solar water heater (flat plate solar collector) working as a brine heater and a vertical flash unit that is attached with a condenser/pre-heater unit. The average accumulative productivity of the system in November, December and January ranged between 1.04 to 1.45 kg/day/m^2. The average summer productivity ranged between 5.44 to 7 kg/day/m^2 in July and August and 4.2 to 5 kg/day/m^2 in June. Junjie et al. [7] studied experimentally the heat and mass transfer properties of static/circulatory flash evaporation, i.e., non-equilibrium fraction (NEF), evaporated mass and heat transfer coefficient. The heat transfer coefficient was redefined as average heat flux released

from unit volume of water film under unit superheat. Results suggested that this coefficient was a time-depended function and a peak value existed in its evolution versus time. Saad et al. [8] proposed and designed a new desalination system for converting sea water into fresh water utilizing the waste heat of internal combustion engines. The desalination process is based on the evaporation of sea water under a very low pressure (vacuum). The low pressure is achieved by using the suction side of a compressor rather than a commonly used vacuum pump. The evaporated water is then condensed to obtain fresh water. The effects of operational variables such as evaporator temperature, condenser temperature, vacuum pressure, and flow rate of both evaporator and condenser on the yield of fresh water are experimentally investigated. It is found that decreasing the vacuum pressure causes a significant increase in the yield of fresh water. It is also found that decreasing the condenser temperature, or increasing the evaporator temperature both lead to an increase in the yield of fresh water. Moreover, increasing the condenser flow rate tends to increase the yield of fresh water. The same trend is attained by increasing the evaporator flow rate. Narayan et al. [9] analyzed the thermodynamic performance of various humidification and dehumidification cycles by way of a theoretical cycle analysis. They propose novel high-performance variations on those cycles. These high-performance cycles include multi-extraction, multi-pressure and thermal vapor compression cycles. The Gained Output Ratio (GOR) of the systems based on these novel cycles excess of 7 and will outperform existing humidification and dehumidification systems.

The solar collector is a convenient and common heater to be used as heat source for many applications such as domestic water heater and desalination purposes. However, the effectiveness of presently solar collector for low-capacity desalination units is low due to some reasons such as the limiting of the thermal conductivity of this working fluid and inefficiency and cost of solar radiation concentrators. Several years ago, the nano-fluid has been found to be an attractive heat transport fluids. It has exhibited a significant potential for heat transfer augmentation relative to the conventional pure fluids. It has been expected to be suitable for the solar water heating systems without severe problems in pipes and with little or no penalty in pressure drop [10]. Asirvatham et al. [11] studied experimentally of steady state convective heat transfer of de-ionized water with a low volume fraction (0.003% by volume) of copper oxide (CuO) nano-particles. The results have shown 8% enhancement of the convective heat transfer coefficient of the nano-fluid even with a low volume concentration of CuO nano-particles. The heat transfer enhancement was increased considerably as the Reynolds number increased. Yousefi et al. [12] investigated experimentally the effect of Al2O3/water nano-fluid, as working fluid, on the efficiency of a flat-plate solar collector. The weight fraction of nano-particles was 0.2% and 0.4%, and the particles dimension was 15 nm. The mass flow rate of nano-fluid varied from 1 to 3 l/min. The results showed that, in comparison with water as absorption medium using the nano-fluids as working fluid increase the efficiency. For 0.2 wt.%, the increased efficiency was 28.3%.

The current work aims to introduce a small-scale hybrid two stages multi-effect air humidification and dehumidification-water flashing evaporation (MEH-SSF) desalination system. A pilot unit was theoretically designed and analyzed to insure;
 - The accurate estimation of the desalted water production improvement,
  - Studying the possible factors and parameters those have an effect on the system production.
  - Studying the heat recovery performance of the system.
  - Studying the effect of nono-fluid as a working fluid for solar water loop on enhancement the system production.

2   SYSTEM PROCESS MODEL

The system consists of two parts. One is two stages of solar humidification–dehumidification unit (HDH), and another is a single-stage flashing evaporation (SSF) unit. A sketch of a hybrid solar desalination process of the two stages of humidification dehumidification and the single stage flashing evaporation unit is shown in Figure (1). Each of the solar humidification–dehumidification unit consists of humidifier, condenser (dehumidifier), and air heater solar collector for first stage only. The first stage of HDH is operated in a forced draft mode by using an air blower and with an open loop for air circulation. A packing is used in the humidifier for efficient humidification of the air. The feed water at (11) is sprayed over the packing in the humidifier. The fresh air at (12) is sucked from atmosphere to enter the humidifier and exit at (13). The brine at (14) is pumped to mixing tank (MT). The saline water at (27) is feed to the dehumidifier to condense the water vapor from the humid air at (13) by using dehumidifier (DE1) and exit at (15). The fresh desalinated water at (24) is collected from the bottom of the condenser. The second stage of HDH is operated in same method of first stage by using feeding and return water closed loop for heat recovery. The feed water at (22) is sprayed over the packing in the humidifier (H2). The air at (15) is discharged to air flat plate solar collector to heat in and exit at (16). The air at (16) is humidified in the humidifier (H2) and exit at (20). The brine at (22) is pumped as feed water again. The saline water at (21) is feed to the dehumidifier (DE2) to condense the water vapor from the air at (20). The fresh desalinated water at (25) is collected from the bottom of the condenser.

The solar SSF unit consists of flashing chamber and condenser. The warm saline water flowed from mixing tank at (5) is reheated in heat exchanger (HHEx) by the heat from water heater flat plate solar collector (SWH) and desalinated in a single-stage flashing distill unit to distill water further. The water at (6) is pumped to flashing chamber to evaporate by flashing. The extracted water vapor on flashing chamber at (10) is flowed to the condenser (C). The saline water at (26) is fed to the flashing unit condenser to condense the water vapor and exit at (9). The desalinated water at (23) is collected from the bottom of the condenser tray, while is rejected from the bottom of the condenser tray. The flashing evaporation depends on the pressure reduction. So, the inside the condenser and flashing chamber is vacuumed by using vacuum pump at (26)).

Then, the saline water exit from condenser (C) at (9), is mixed with rejected brine water from humidifier (H1) at (14), in mixing tank as will as is further preheated the feed water to (5) and (11) and the saline water exit from dehumidifiers (DE1) and (DE2) at (17) and (18) respectively are drained. A part of saline water in mixing tank (MT) is flowed to helical heat exchanger (HHEx) to backup water inside the closed loop of saline water flow between the flashing chamber and heat exchanger (HHEx) at (5) while the rest is drained at (8). As mentioned above; the mixing tank is used to improve the system performance due to its dual effect in energy saving for both HDH and SSF systems, where the heat recovery from the rejected hot water is increased. Humidification-dehumidification cycle is shown in Figure (2) on psychrometric chart for HDH unit. Figure (3) shows the evaporation and condensation processes on T-s diagram for SSF unit. Description of the equipments of the system is shown in Table (1).

Figure 1. HDH-SSF process schematic diagram.
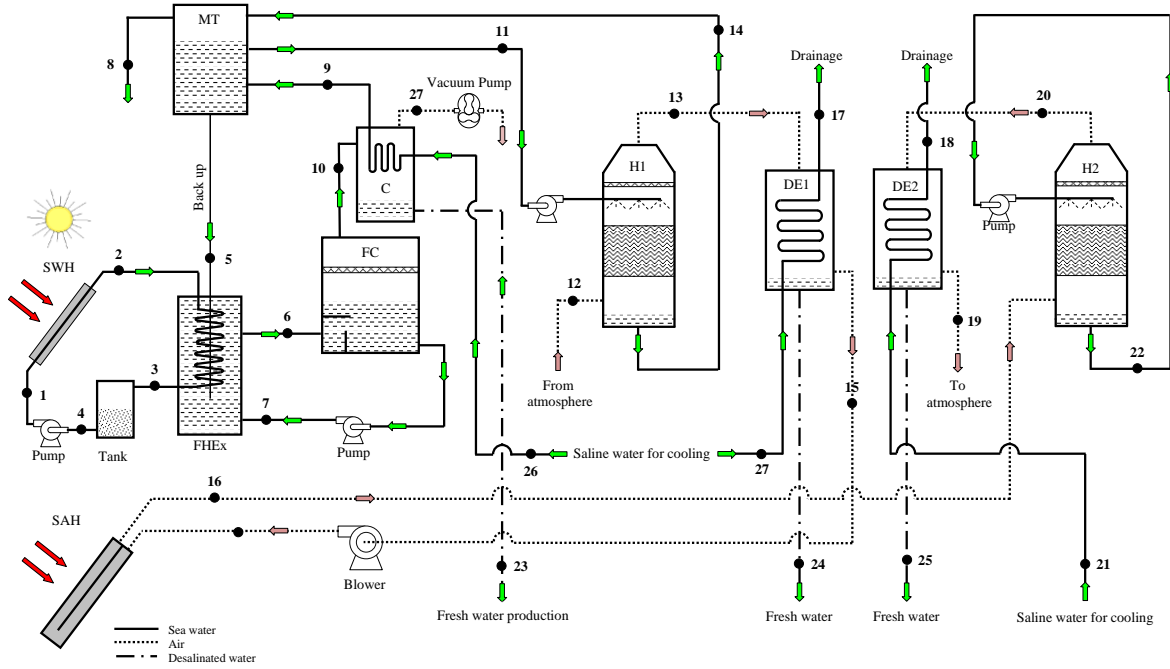
1.	MT:	Mixing tank		5.	C:	Flashing unit condenser
2.	SWH:	Solar water heater		6.	FC:	Flashing chamber
3.	Hex:	Heat exchanger		7.	H:	Humidifier
4.	SAH:	Solar air heater		8.	DE:	Dehumidifier

Table (1): System technical specifications data used for the simulation

Technical specifications and operation data	Value
Solar water heater (SWH)	
Total aperture area, m^2	7
Glass type low iron glass thickness, mm	3
Collector insulation Fiberglass sides thickness, mm	30
Fiberglass back thickness, mm	50
Solar air heater (SAH)	
Total aperture area, m^2	1.415
Glass type low iron glass thickness, mm	3
Collector insulation Fiberglass sides thickness, mm	30
Fiberglass back thickness, mm	50
Humidifier (H)	
Size, m	0.45 ID×0.8
Packing bed: Raschig rings (packing void)	0.92
Dehumidifier (C2)	
Size, mm	186×144×260
Exchange surface area, m^2	0.1
Heat exchanger (Hex)	
Exchange surface area, m^2	1.37
Flashing chamber (FC)	
Size, m	0.2×0.5×0.5
Brine pool height, m	0.10
Condenser of flashing unit (C1)	
Condenser surface area, m^2	0.2

According to the above selection characteristics, Table (2) is summarized the specifications of the tested nano-fluid as-received were taken and some representative data. The nano-particle material that used for investigation in the present experimental work is procured from a China based company (Qinhuangdao Taiji Ring Nano-Products Ltd).

Table (2): Specifications of tested nano-fluid.

| Parameters	Value / Type
Nano particle material	
Nano particle material	Al_2O_3
Product model (according to data sheet form supplier)	AL-01
Purity of nano particle material	99.9%
Appearance	White
Nano particle size (diameter) , d_{np} (m)	30×10^{-9}
Specific surface area, (m^2/g)	160
Volume density, (g/ cm^3)	0.916
Density, ρ_{np} (kg/m^3)	3910
Specific heat, $C_{p,np}$ (J/kg.K)	880
Thermal conductivity, K_{np} (W/m.K)	36
Crystal Form	γ
Characteristics	Insoluble
Particle shape	sphere
Nano-fluid	
Base fluid	Distilled water
Dispersion condition	Agitation
Dispersant agent	SDBS 1.0 wt. %
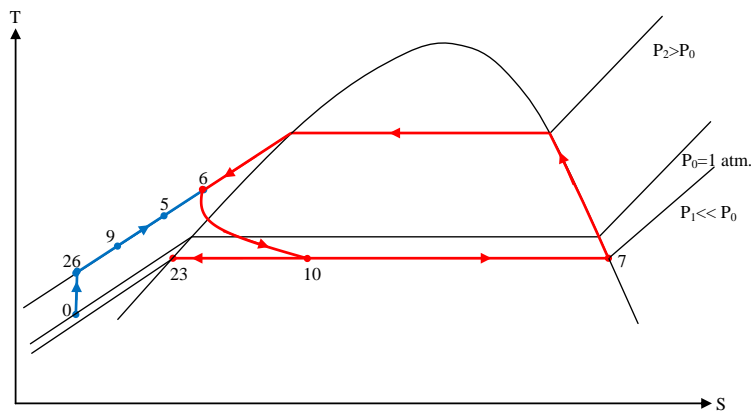
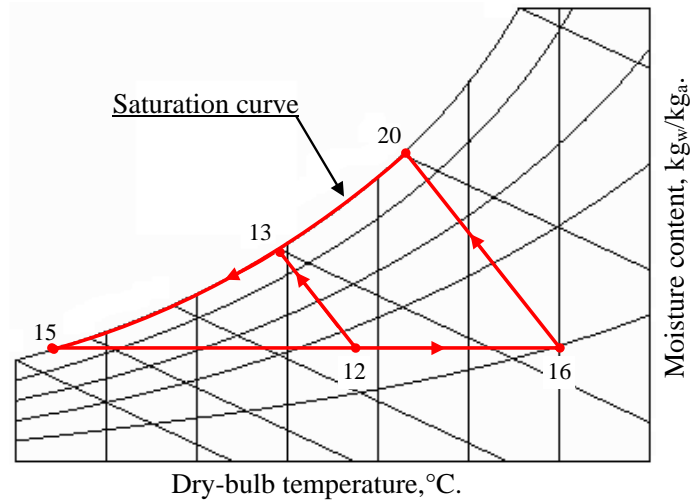**Figure 2. T-s diagram for the evaporation and condensation processes.**

Figure 3. Change of state of process air through the HDH unit cycle on psychrometric chart.

3 SYSTEM MATHEMATICAL MODELING

The mathematical model in the steady-state regime allows determining the coupling equations between the water temperature, the humid air temperature and water content inside each component. The water salinity will be considered. The energy balance equation can be written for the entire system in the following manner, by taking input energy terms equal to output energy terms. For the energy balance and governing equations for each of the system components the following assumptions are considered:

1. The system is behaved in a quasi-steady-state manner and one dimensional; i.e. the variables, while varying from hour to hour, are considered constant during every hour of analysis and the unsteady terms in the governing equations are neglected,
2. Heat losses from the edges of the solar air and water heaters, mixing tank, humidifier, dehumidifier and flashing unit to the ambient are neglected (i.e. the heat exchanger outside walls are adiabatic),
3. The convection effects between the glass covers of solar air heater are neglected.
4. Negligible conduction resistance in glass covers of solar collectors,
5. The absorption of solar radiation in the cover is neglected insofar as it affects loss from the solar air collector,
6. Air is an ideal gas,
7. The temperature distribution over every cross section in the mixing tank is uniform,
8. Air temperature varies linearly in the flow directions,
9. Flow that is laminar or turbulent is fully developed,
10. The flash chamber is in equilibrium with the brine leaving the stage,
11. The distillate vapor always condenses completely,
12. The flow of non-condensable is negligible,

The details description and the theoretical modeling are clarified in Kabeel and El-said

3.1 Humidifier modeling

The formulation of the mathematical model is obtained by applying the thermal and mass transfers on an element of volume of height *dy*. For the humidifier packing bed cross-sectional area $A_{cs,ev}$ and $H_{p,ev}$ height, the dry air mass flux is:

$$M_{a,ev} = \frac{\dot{m}_{a,ev}}{A_{cs,ev}} \quad\text{...} \quad (1)$$

And the corresponding mass flux of water flowing parallel with the air is

$$M_{w,ev} = \frac{\dot{m}_{w,ev}}{A_{cs,ev}} \quad\text{...} \quad (2)$$

If $a_{H,,ev}$ and $a_{M,ev}$ are the area of heat transfer and mass transfer surface per unit of packing volume, respectively, the total surface areas for heat and mass transfer are:

$$A_{H,ev} = H_{P,ev} a_{H,ev} A_{cs,ev} \quad \text{and} \quad A_{M,ev} = H_{P,ev} a_{M,ev} A_{cs,ev} \quad\text{..............................} \quad (3)$$

The basic equations for the process occurring in the differential length *dy* can be written as following.

Mass balance for humid air and water:

The mass balance equation of the amount of evaporated water into air yields:

$$\frac{dM_{w,ev}}{dy} = k_{a,ev} \rho_{a,ev} a_{H,ev} \left(\omega_{i,ev} - \omega_{a,ev} \right) \text{...} \quad (4)$$

Where $k_{a,ev}$ is air-side mass transfer coefficient (from air to interface)

Heat transfer to air

The sensible heat transfer between liquid and gas within the element *dy*, is given by:

$$\frac{dT_{a,ev}}{dy} = \frac{h_{a,ev} a_{H,ev} \left(T_{i,ev} - T_{a,ev} \right)}{M_{a,ev} C_{P,ha,ev}} \quad\text{...} \quad (5)$$

Where:

$$C_{p,ha,ev} = C_{p,a,ev} + \omega_{a,ev} C_{p,v,ev} \text{...} \quad (6)$$

Energy balance for water:

Equating the energy at water side leads to:

$$\frac{dT_{w,ev}}{dy} = \frac{h_{w,ev} a_{M,ev} \left(T_w - T_i \right)}{M_{w,ev} C_{p,w,ev}} \quad\text{...} \quad (7)$$

Energy balance for humid air:

$$M_{a,ev}C_{p,ha,ev}\frac{dT_{a,ev}}{dy}+M_{a,ev}\lambda_{fg,ev}\frac{d\omega_{a,ev}}{dy}=h_{a,ev}a_{H,ev}\left(T_{i,ev}-T_{a,ev}\right)+$$
$$k_{a,ev}\rho_{a,ev}a_{M,ev}\lambda_{fg,ev}\left(\omega_{i,ev}-\omega_{a,ev}\right) \quad \text{............} \quad (8)$$

Salt mass balance for water:

The overall salt mass balance assumes that the distillate water is salt free. The balance equations are given by:

$$x_{w,in}\dot{m}_{w,in}=x_{w,o}\dot{m}_{w,o} \quad \text{..} \quad (9) \quad \mathbf{3.2}$$

Dehumidifier modeling

For a typical element *dy*, the humid air and the condensed water film flow between the tubes and the cooled water flows inside the tubes in Y direction.

Energy balance for cooling water:

$$\frac{dT_{w,co}}{dy}=\frac{N_{coil,co}\pi d_{tube,in,co}U_{L,co}\left(T_{a,co}-T_{w,co}\right)}{\dot{m}_{w,co}C_{p,w,co}} \quad \text{......................................} \quad (10)$$

Mass balance for humid air:

$$\frac{d\omega_{a,co}}{dy}=N_{coil,co}\pi d_{tube,o,co}\left[\frac{k_{co}\left(\omega_{a,co}-\omega_{i,co}\right)}{\dot{m}_{a,co}}\right] \quad \text{...............................} \quad (11)$$

Energy balance for humid air:

$$C_{p,ha,co}\frac{dT_{a,co}}{dy}+\lambda_{fg,co}\frac{d\omega_{a,co}}{dy}=\frac{N_{coil,co}\pi d_{tube,o,co}}{\dot{m}_{a,co}}\left[\begin{array}{l}h_{a,co}\left(T_{a,co}-T_{i,co}\right)+\\k_{co}\lambda_{fg,co}\left(\omega_{a,co}-\omega_{i,co}\right)\end{array}\right] \quad \text{...............} \quad (12)$$

Condensation production:

The condensation rate is determined using an algebraic equation that relates the variation of the water content along the height of the dehumidifier:

$$d\dot{m}_{dis}=\dot{m}_{a,co}d\omega_{a,co} \quad \text{...} \quad (13)$$

3.3 Flat plate solar water heater modeling

Flat plate solar collector is used to heat water. The proof of governing equations on the solar collector energy analysis is not included to have a detail note [13]. The useful heat gain (q_u) by the working fluid is

$$q_u=\dot{m}_{f,wc}c_{p,f,ac}\left(T_{o,wc}-T_{in,wc}\right) \quad \text{.......................................} \quad (14)$$

The Hottel–Whillier equation for the useful heat gain (q_u) of a flat plate solar collector system, considering the heat losses from the solar collector to the atmosphere, is

$$q'_u = W_{tube} F' \left[S - U_{L,wc} \left(T_{f,wc} - T_{am} \right) \right] \quad \text{..} \quad (15)$$

Where the collector efficiency factor (F') is given by:

$$F' = \frac{1}{U_{L,wc} W_{tube} \left\{ \dfrac{1}{U_{L,wc} \left[d_{wc,o} + F \left(W_{tube} - d_{wc,o} \right) \right]} + \dfrac{1}{C_{bo}} + \dfrac{1}{h_{f,wc,in} \pi d_{wc,in}} \right\}} \quad \text{................} \quad (16)$$

In Eq. (15) the radiation absorbed flux by unit area of the absorber plate (S) is defined as

$$S \cong 0.97 \tau_{g_c} \alpha_{ap} I_T \quad \text{...} \quad (17)$$

Consider an infinitesimal length (dy) of the tube. The useful energy delivered to the fluid is $q'_u dy$. Under steady-state conditions, an energy balance for (N) tubes gives:

$$q'_u dy + \frac{\dot{m}_{wc}}{N_{wc,tube}} C_{p,wc} T_{wc} - \frac{\dot{m}_{wc}}{N_{wc,tube}} C_{p,wc} \left(T_{wc} + \frac{dT_{wc}}{dy} dy \right) = 0 \quad \text{..........................} \quad (18)$$

Dividing through by (dy), finding the limit as (dy) approaches 0, and substituting Eq. (18) results in the following differential equation:

$$\dot{m}_{wc} C_{p,wc} \frac{dT_{wc}}{dy} - N_{wc,tube} W_{tube} F' \left[S - U_{L,wc} \left(T_{f,wc} - T_{am} \right) \right] = 0 \quad \text{.........................} \quad (19)$$

Assuming variables F', $U_{L,wc}$, and C_p to be constants and performing the integration gives:

$$\ln \left(\frac{T_{wc,o} - T_{am} - \left(S / U_{L,wc} \right)}{T_{wc,in} - T_{am} - \left(S / U_{L,wc} \right)} \right) = -\frac{N_{wc,tube} W_{wc} L_{coil,wc} F' U_{L,wc}}{\dot{m}_{wc} C_{p,wc}} \quad \text{.........................} \quad (20)$$

Where

$$A_{wc} = N_{wc,tube} W_{tube} L_{tube,wc}$$

Then

$$T_{wc,o} = \left[T_{wc,in} - T_{am} - \left(S / U_{L,wc} \right) \right] \left[\exp \left(-\frac{A_{wc} F' U_{L,wc}}{\dot{m}_{wc} C_{p,wc}} \right) \right] + T_{am} + \left(S / U_{L,wc} \right) \quad \text{.........} \quad (21)$$

3.4 Solar air heater modeling

The top layer of glass cover:

$$U_t \left(T_{g1} - T_{am} \right) = h_{r,g2-g1} \left(T_{g2} - T_{g1} \right) \quad \text{...} \quad (22)$$

The lower layer of glass cover:

$$h_{c,f1-g2}\left(T_{f1}-T_{g2}\right)+h_{r,p-g2}\left(T_p-T_{g2}\right)=h_{r,g2-g1}\left(T_{g2}-T_{g1}\right) \quad\quad (23)$$

The heat absorbing plate:

$$S=h_{c,p-f1}\left(T_p-T_{f1}\right)+h_{c,p-f2}\left(T_p-T_{f2}\right)+h_{r,p-g2}\left(T_p-T_{g2}\right)+h_{r,p-b}\left(T_p-T_b\right) \quad\quad (24)$$

Insulation bottom board:

$$U_b\left(T_b-T_{am}\right)=h_{r,p-b}\left(T_p-T_b\right)+h_{c,f2-b}\left(T_{f2}-T_b\right) \quad\quad (25)$$

The heat transfer capacity between heat-absorbing plate and the air of the top channel (q_{u1}):

$$q_{u1}=h_{c,p-f1}\left(T_p-T_{f1}\right)+h_{c,f1-g2}\left(T_{g2}-T_{f1}\right) \quad\quad (26)$$

The heat transfer capacity between heat-absorbing plate and the air of the lower channel (q_{u2}):

$$q_{u2}=h_{c,p-f2}\left(T_p-T_{f2}\right)+h_{c,f2-b}\left(T_b-T_{f2}\right) \quad\quad (27)$$

Based on equation (26) and (27) (q_u) the heat transfer capacity between the air and heat absorbing plate can be calculated by the following formula (q_u):

$$q_u=h_{c,p-f1}\left(T_p-T_{f1}\right)+h_{c,f1-g2}\left(T_{g2}-T_{f1}\right)+h_{c,p-f2}\left(T_p-T_{f2}\right)+h_{c,f2-b}\left(T_b-T_{f2}\right) \quad\quad (28)$$

And

$$q_u=\dot{m}_a c_{p,a}\left(T_{fo}-T_{fi}\right) \quad\quad (29)$$

By combination Eq. (28) and Eq. (29) gives:

$$\dot{m}_a c_{p,a}\left(T_{fo}-T_{fi}\right)=h_{c,p-f1}\left(T_p-T_{f1}\right)+h_{c,f1-g2}\left(T_{g2}-T_{f1}\right)+h_{c,p-f2}\left(T_p-T_{f2}\right)$$
$$+h_{c,f2-b}\left(T_b-T_{f2}\right) \quad\quad (30)$$

3.5 Single stage flashing unit modeling

The mathematical model for the single flash unit is simple and it includes total mass and salt mass balances, rate equations for the heat transfer units, as well as energy balances for the condenser.

Flashing pool model

Total mass and salt mass balances:

$$\dot{m}_{fw,fu}=\dot{m}_{b,fu}+\dot{m}_{dis,fu} \quad\quad (31)$$

$$x_{fw,fu}\,\dot{m}_{fw,fu}=x_{b,fu}\,\dot{m}_{b,fu} \quad\quad (32)$$

Eq. (32) assumes that the salt concentration, (x_{dw}), in the formed vapor is zero.

Energy balance:

The energy balance for the flashing brine is expressed as follows:

$$\dot{m}_{fw,fu}\, i_{fw,fu} = \dot{m}_{b,fu}\, i_{b,fu} + \dot{m}_{dis,fu}\, \lambda_{v,fu} \quad\ldots\ldots\ldots\ldots\ldots\ldots\ldots\ldots\ldots\ldots\ldots\ldots\ldots\ldots \quad (33)$$

Condenser tube bundle model

Energy balances:

$$\dot{m}_{dis,fu}\, \lambda_{v,fu} = \dot{m}_{cwfu}\left(i_{cwo,fu} - i_{cwin,fu}\right) + \dot{m}_{dis,fu}\, i_{dis,fu} \quad\ldots\ldots\ldots\ldots\ldots\ldots\ldots\ldots\ldots \quad (34)$$

The heat transfer rate equation for the condenser is

$$\dot{m}_{cwfu}\left(i_{cwo,fu} - i_{cwin,fu}\right) = \dot{m}_{cwfu}\, C_{p,cwfu}\left(T_{cwo,fu} - T_{cwin,fu}\right) = U_{cafu}\, A_{cafu}(LMTD)_{cafu} \quad\ldots \quad (35)$$

From Eq. (34) and after a few steps of simplification; the following equation is obtained:

$$(1-C)T_{cwin,fu} + C\, T_{v,fu} = T_{cwo,fu} \quad\ldots\ldots\ldots\ldots\ldots\ldots\ldots\ldots\ldots\ldots\ldots\ldots\ldots\ldots \quad (36)$$

Where

$$C = 1 - e^{NTU} \quad \text{and} \quad NTU = -\frac{U_{cafu}\, A_{cafu}}{\dot{m}_{cwfu}\, C_{p,cwfu}}$$

For the equilibrium correlation; the relation between the outlet brine temperature (T_b) and the condensation temperature of the vapor, (T_v). is presented by following equation [14].

$$T_{v,fu} = T_{b,fu} - NEA - BPE \quad\ldots\ldots\ldots\ldots\ldots\ldots\ldots\ldots\ldots\ldots\ldots\ldots\ldots\ldots\ldots \quad (37)$$

4   MATHEMATICAL PROGRAMING MODEL

   The main constraints of the mathematical programming model of the solar HDH-SSF system were presented in the previous section. Algebraic equations are used in to the model in original form. But for applying the differential equations, firstly they should be formed as algebraic equations using the forward finite difference method to obtain the required values for air and water temperature, air humidity, flow rates of air and water. So, each of humidifier and dehumidifier is divided into $j = 10$ equal intervals or elements, the differential equations are expressed as a set of nonlinear algebraic equations. For the iteration procedure, the inlet water temperature of the solar water heater and the inlet air temperature of the solar air heater are guessed. The calculation procedure then marches along the solar water heater, solar air heater, humidifier, dehumidifier and flashing chamber. The outlet temperature of each unit is taken as the input for the next one. Finally, the outlet water and air temperatures are compared with the guessed inlet temperatures. The water and air physical properties are calculated as functions of temperature. The values of solar intensity is calculated numerically through the day and used as initial conditions for solution. A computer code in MATLAB® is prepared to solve the nonlinear set of equations of several variables using Gauss–Seidel iteration method. The programming takes into account that the air flow is in a counter direction of water flow. The temperature of air and water as well as the air humidity ratio is obtained at each segment in order to calculate the temperature distribution along the flow direction. Iterative procedure is followed for each segment and the solution is assumed to converge until the following inequality is valid:

$$\left|T^e - T^g\right| \le 0.01 \quad\ldots\ldots\ldots\ldots\ldots\ldots\ldots\ldots\ldots\ldots\ldots\ldots\ldots\ldots\ldots\ldots \quad (38)$$

The iteration is continued until the physical properties of water and air are obtained at each segment as a function of the mean temperature in any iteration.

5   ECONOMIC ANALYSIS

It is of great interest to study economically the current desalination unit because a system may be technically very efficient. However, it may not be economic; the cost of water production may be too high. The current economic analysis is conducted to determine both the cost of the water product. The total cost of ownership (TCO) concept was adopted in the analysis. The TCO concept includes different types costs like; the fixed investment costs, the production costs, the internal rate of return on investment, the operating costs, the energy costs and some other economic parameters. The investment cost of each component constituting the system is presented in Table (4).

Table 4: Capital investment cost for HDH-SSF plants (the installation costs are included).

Item Description	Cost
Packed bed humidifier	133 US$
Dehumidifier	70 US$
Solar water heater	850 US$
Solar air heater	100 US$
Helical coil heat exchanger	80 US$
Flashing evaporation unit	85 US$
Mixing tank	25 US$
Tanks	80 US$
Pumps and blowers	345 US$
Control devices	80 US$
Pipes, fittings	35 US$
Accessories	24 US$
Nano-particle kg.	80US$

The costs are varied from country to country depending on a lot of factors like; the labor costs, the site of the country (transportation costs), the local currency of the country and its relation to the international currency (USD).
  Many assumptions are considered during the simulations as;
-   Some aspects of investments are not included, like the lower probability of the systems to shutdown or proven process control is used for the desalination plants.

- All the environmental costs and the possible environmental impacts of investments are not considered.
- Costs that are not included in the capital cost estimates are: cost of drinking water conveyance facilities outside the plant boundary and interest charges during construction.
- The operating costs include the amortization or fixed charges, operating and maintenance costs and energy costs.
- A zero net salvage value is recorded (for land, buildings, equipment, etc.) and a continual replacement of such capital items into perpetuity.
- The capital cost estimate for all options is based on local prices for the equipment and no import taxes or duties are considered.
- The capital costs also include all costs for engineering, transportation, construction as well as commissioning.
- The operating and the maintenance costs are 20% of plant annual payment [14].
- Zero pretreatment costs.
- The interest rate is 5%.
- The plant life expectancy is 20 years.
- The plant availability (*f*) is 90% [14].

The calculation methodology is based on; the salvage value of the units will be zero at the end of the amortization period. The produced fresh water can be blended with the raw water to achieve adequate potable water salinity (500 ppm according to the WHO recommended value). The amount of water that can be blended will depend on the blend water quality and the goals of the final required product water quality. For 1000 ppm brackish water, the simple mass balance results indicated that, the total produced potable water will be two times the distilled water produced, where the potable water salinity is 500 ppm. The total cost of ownership is calculated from the following relation;

$$TCO = C_{op} + C_{main} + C_{fix} \quad \text{………………………………………...………….…..…} \quad (39)$$

Where;

C_{op} is the cost of operation; it includes the energy, the operating personnel, and the handling of raw materials.

C_{main} is the cost of maintenance; it includes the maintenance personnel, the maintenance facility cost, the test equipment, the maintenance support and handling cost, the maintenance spares and repair parts.

C_{fix} is the fixed charges cost, it is calculated as follows;

$$C_{fix} = a \times C_c \quad \text{…………………………………………………........….………..…} \quad (40)$$

Where amortization factor (***a***), which is given by [15]:

$$a = \frac{i(1+i)^n}{(1+i)^n - 1} \quad \text{……………………………..………………………………....….…} \quad (41)$$

i, is the annual interest rate (%) and *n* is the plant life time.

C_c is the capital cost; hence the product water coat is calculated from the following relation assuming 365 working days.

$$C_{prod} = \frac{TCO}{f \times CA \times 365} \quad \text{...} (42)$$

The cost of energy consumption; the electrical energy for the water pumps were 17.88 kWh/m$^{3.}$ The efficiency values for both the water pump and the air blower were 80% when calculating the consumed energy [16].

During the current study, many concerns were considered to cover the probable uncertainties like; the introduced costs are based on both a real purchasing prices and some previously mentioned assumptions. Also; all costs are adopted in a recent year (2012) in dollars, the capital cost estimate for all options was based on the Egypt local prices for the different equipments, there is no import taxes or duties are considered, finally an annual inflation rate of 5% is considered for the prices change in Egypt. In the present study, the two desalination plants modes are considered based on a thermal solar heat source only.

6   SYSTEM PERFORMANCE

In reviewing the literature on low temperature desalination unit's thermal efficiency many parameters can be found, and often relate to the rating of desalination plant performance, in terms of the volume of water produced for the energy consumed. The most commonly encountered performance metrics for desalination systems are the Gained Output Ratio (GOR), which is discussed below. Another performance parameter is specific work which can measure the auxiliary electricity consumed. So, the system performance of the HDH-SSF system can be evaluated in these terms.

6.1 Gained Output Ratio

The Gained Output Ratio (GOR) is a dimensionless ratio, used for thermal desalination processes, defined either as an energy ratio or a mass ratio. As an energy ratio it is usually defined as the ratio of the latent heat of evaporation of the water produced to the net heat input to the cycle. This parameter is, essentially, the effectiveness of water production, which is defined as an index of the amount of the heat recovery affected in the system [17]:

$$GOR = \frac{\Delta h_{evap} \dot{m}_{dis}}{\dot{Q}_{in}} \quad \text{..} (43)$$

The GOR does not take into account any system efficiencies external to the desalination plant, such as heat losses through piping from the heat source.
   The total GOR of the hybrid desalination system is calculated by [18]:

$$GOR_{sys} = GOR_{HDH} + GOR_{SF} \text{..} (44)$$

5.2 Specific work

Specific work (SW) is the ratio of the auxiliary electricity consumed by blowers and pumps used for air and water circulation per unit amount of water produced in the   HDH-SSF system [19]:

$$SW = \frac{\dot{W}_{aux}}{\dot{m}_{dis}} \quad \ldots\ldots\ldots\ldots\ldots\ldots\ldots\ldots\ldots\ldots\ldots\ldots\ldots\ldots\ldots\ldots\ldots\ldots \quad (45)$$

7   RESULTS AND DISCUSSION

There are seven operation parameters (feed water flow rate of SSF unit, feed water flow rate of HDH units, cooling water flow rate of SSF unit, cooling water flow rate of HDH units, air flow rates, cooling water temperatures, nano-particle volume fraction) have a direct impacts on the system overall productivity. There are other parameters can affect in the unit productivity such as feed water salinity and wind speed. But these parameters has small effects on the unit productivity, Nafey et al. [3,4], Yamal and Solmus [20].The numerical results that presented in this section are computed for 10 hours of operation time period start at 07:00 AM until 17:00 PM on August for Tanta city. The accumulative productivity of both methods (HDH and SSF) theoretically at the mentioned times and date according to operation conditions. The solar radiation rate is measured experimentally according to location and weather conditions of Tanta city site. The values of the solar radiation on a horizontal surface and measured values ambient temperature during the average day of August are given in Figure (4).
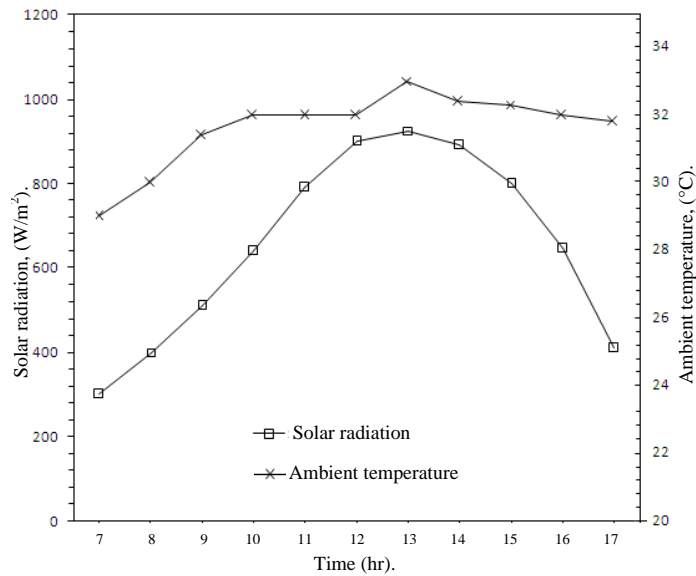

Figure 4. Variation of solar radiation and ambient temperature during the average day time.

7.1. System productivity

Figure (5) shows the accumulative fresh water production in the day time per unit air and water collectors' areas. According to the Figure (5), it can be seen that the fresh water system production increase with the solar intensity strengthening and the freshwater production reduce with the solar intensity weakening. The daily water production of the system is about 112.5 kg/day.

7.2. Feed water mass flow rate of SSF unit effect

Variations of system productivity for different feed water mass flow rate of SSF unit and solar water heater working fluid (distilled water) mass flow rate are presented in Figure (6). At constant solar water heater working fluid mass flow rate, it shows that the productivity of the system increases with increasing values of feed water mass flow rate of SSF unit. These may be explained as follows; by increasing the flow rate of the SSF unit the rejected brine temperature will increase feed water temperature and then increase the productivity of the unit.
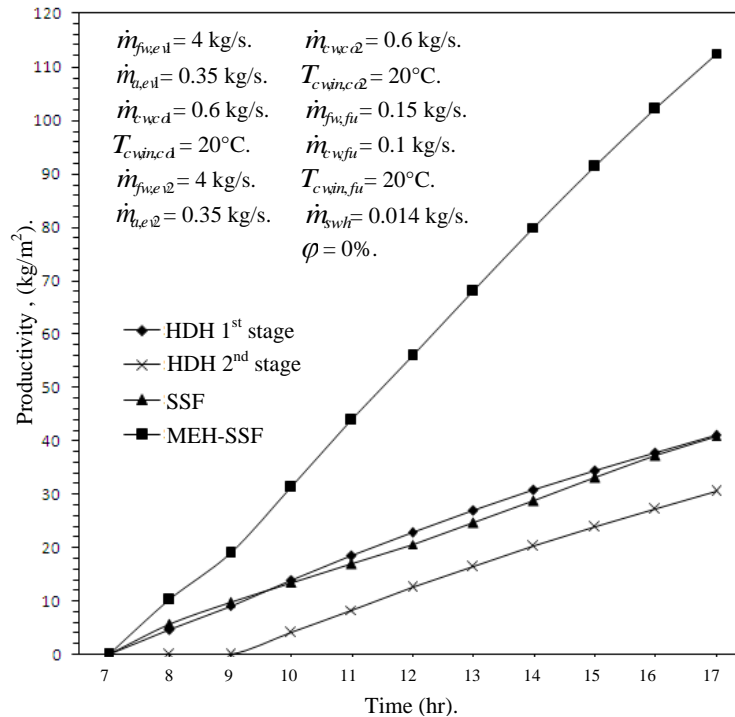
Figure 5. Productivity and solar radiation during day hours.

The results in Figure (6) are shown also that the increasing of the mass flow rate of working fluid (distilled water) of solar water heater gradually, the system productivity will increase while the working fluid outlet temperature at (2) (see Figure (1)) will gradually decrease. The system productivity will increase against the increasing of mass flow rate of working fluid of solar water heater till the feed reaches a certain value then by increasing the mass flow rate the productivity will decrease because of the decreasing in working fluid outlet temperature the solar water heater will become has effect more than increasing of heat capacity occurred by increasing of the mass flow rate of working fluid.

7.3. Feed water mass flow rate of HDH units effect

Figures (7) and (8) present the effect of the humidifier (H1) and (H2) feed water mass flow rate on the system productivity. It shows that the productivity of the system increases with increasing value of inlet water mass flow rate of HDH units. All of these findings may be explained as follows; at a constant air mass flow rate, when the water mass flow rate is increased, the heat transfer rate between air and water will improve. This means that, the evaporation rate is increased. So, the moisture content of the air leaving the humidifier increases.
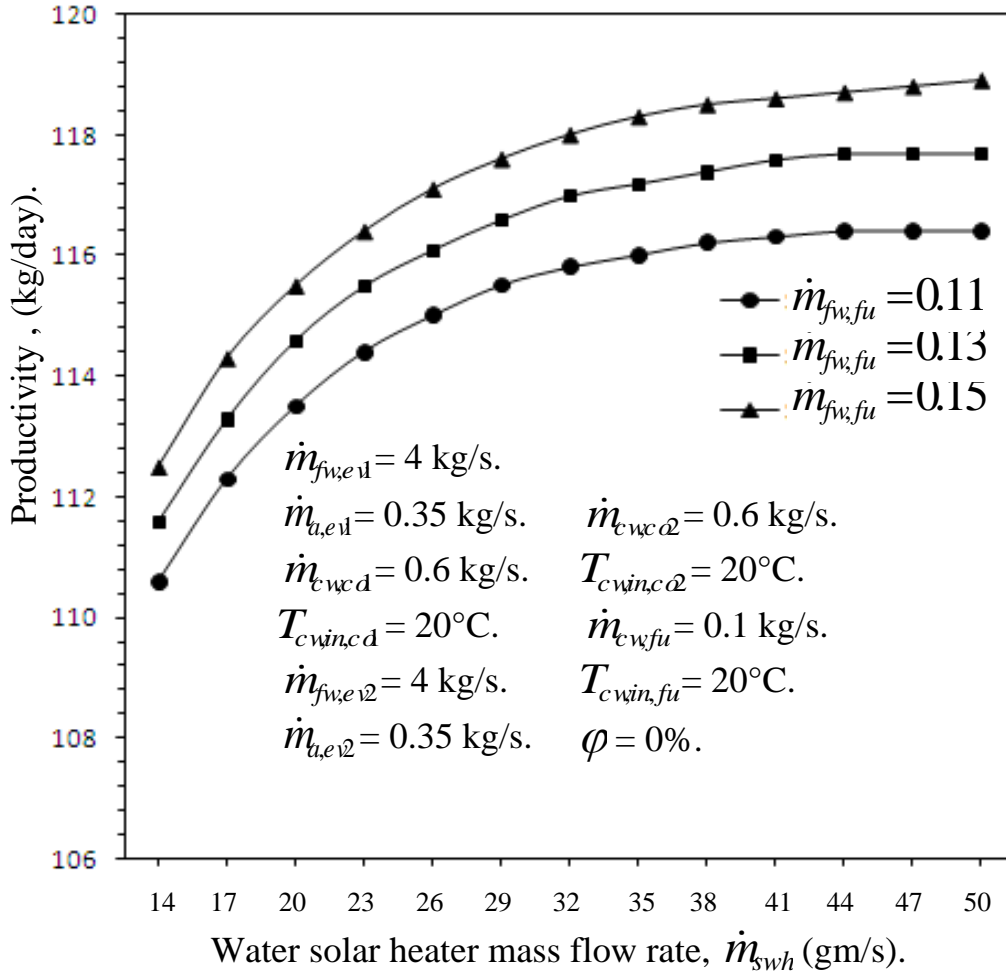
Figure 6. Variations in system productivity as a function of feed water mass flow rate of SSF unit at different values of

For the HDH unit, the temperature of the air at the outlet of the solar air heater decreases when the air mass flow rate is increased. In addition, at a constant water mass flow rate, temperature of the air leaving the humidifier decreases, and it gets closer to the wet-bulb temperature of the air at the inlet of the humidifier. Consequently, the rate of vaporization in the humidifier decreases then, the productivity of the system is reduced; however, on the contrary, it can be observed that the effect of the inlet air mass flow rate on the system productivity increases by increasing the air mass flow rate. The reason behind this behavior can be explained as follows; the increasing of the air flow rate increases the mass and heat transfer coefficients inside the humidifier, which increases the rate of vaporization of water and, hence, the unit productivity. In present studied case the second impact of air mass flow rate increasing is more effect on system productivity.
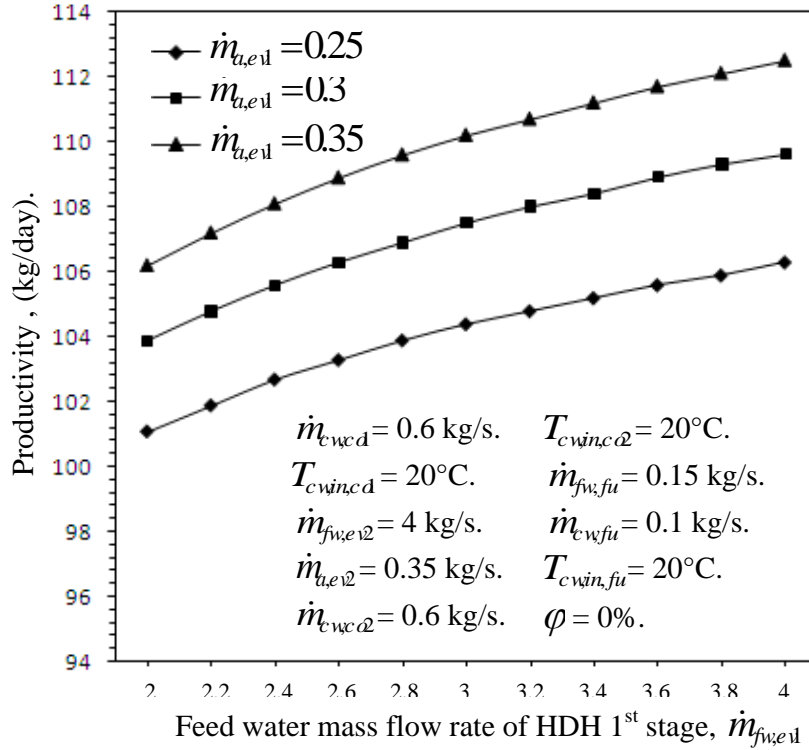
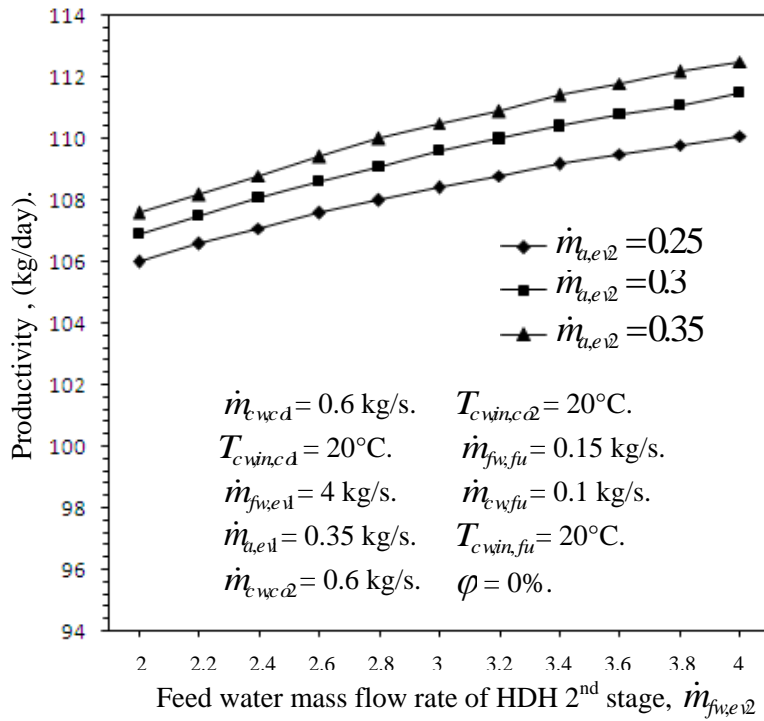**Figure 7. Variations in system productivity as a function of feed water mass flow rate of HDH 1st stage.**

Figure 8. Variations in system productivity as a function of feed water mass flow rate of HDH 2nd

stage.

7.4. Cooling water mass flow rate of SSF unit effect

The effect of the cooling water mass flow rate of SSF unit on the system productivity is shown in Figure (9). By increasing the cooling water mass flow rate, significant drop in the surface temperature of the condenser tubes can be achieved which results in an increase of the rate of the condensation of the water vapor on the condenser tubes surface then, the system gives higher productivity. On the other hand, the increasing the cooling water temperature, rise in the surface temperature of the condenser tubes can be achieved, which results in a decrease of the rate of the condensation of the water vapor on the condenser tubes surface and then lead to lower productivity. The results showed that, the water production of SSF unit increases with the decreasing of the cooling water inlet temperature and/or increasing of mass flow rate of cooling water. Moreover, the impact of decreasing of cooling water inlet temperature is more effect on system productivity than increasing of cooling water mass flow rate.
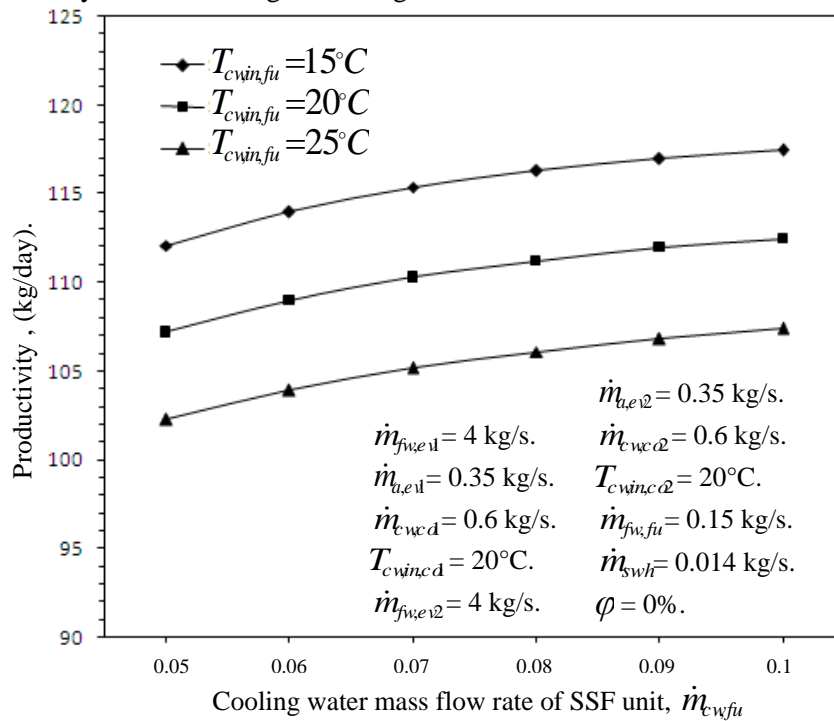

Figure 9. Variations in system productivity as a function of cooling water mass flow rate of SSF unit.

7.5. Cooling water mass flow rate of HDH units effect

The effect of the cooling water mass flow rate of HDH units on the system productivity is shown in Figures (10) and (11) for dehumidifier (DE1) and (DE2). It is shown that the productivity of the HDH unit is not affected by change the value of cooling water mass flow rate. On the contrarily, the decreasing of cooling water inlet temperature has a high significance effect on system productivity.
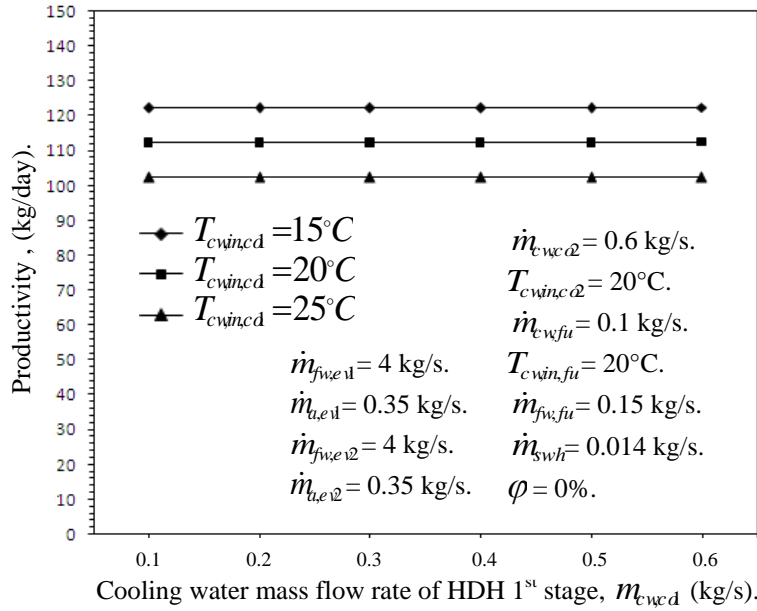
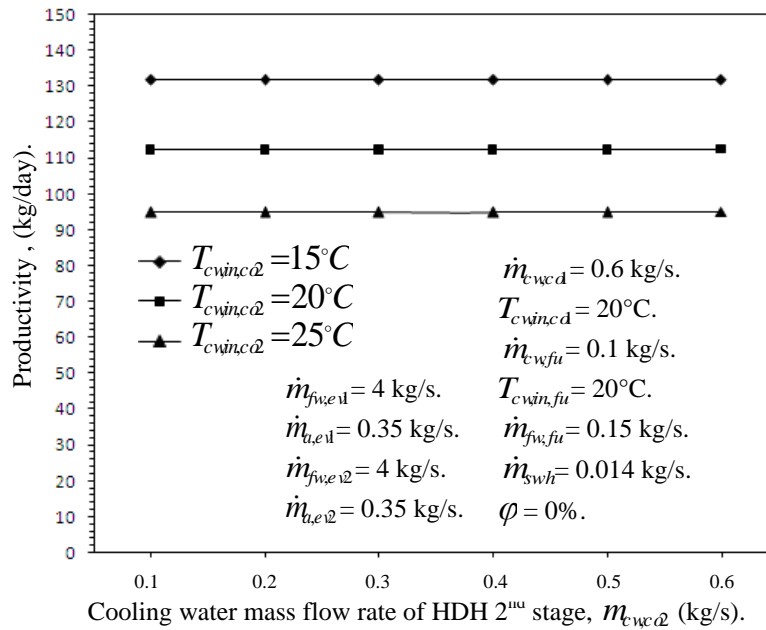**Figure 10. Variations in system productivity as a function of cooling water mass flow rate of HDH 1st stage.**

Figure 11. Variations in system productivity as a function of cooling water mass flow rate of HDH 2nd stage.

7.6. Nano-particles volume fraction and solar collector working fluid volume flow rate effects

The variations in system productivity as a function of solar collector water mass flow rate

nano-particles volume fraction on the system productivity is shown in Figure (12). It is shown that the productivity of the system increases with increasing nano-particles volume fraction. These may be explained as follows; by increasing of nano-particle volume fraction will increase the working fluid thermal conductivity, density and viscosity which increasing the solar heat gain with increasing or decreasing of heat transfer rate in helical heat exchanger as well as causes increasing or decreasing of feeding water temperature respectively. For present case, the system productivity will increase against the increasing of solar collector working fluid mass flow rate because of the decreasing in working fluid outlet temperature the solar water heater will become has effect more than increasing of heat capacity occurred by increasing of the mass flow rate of working fluid.
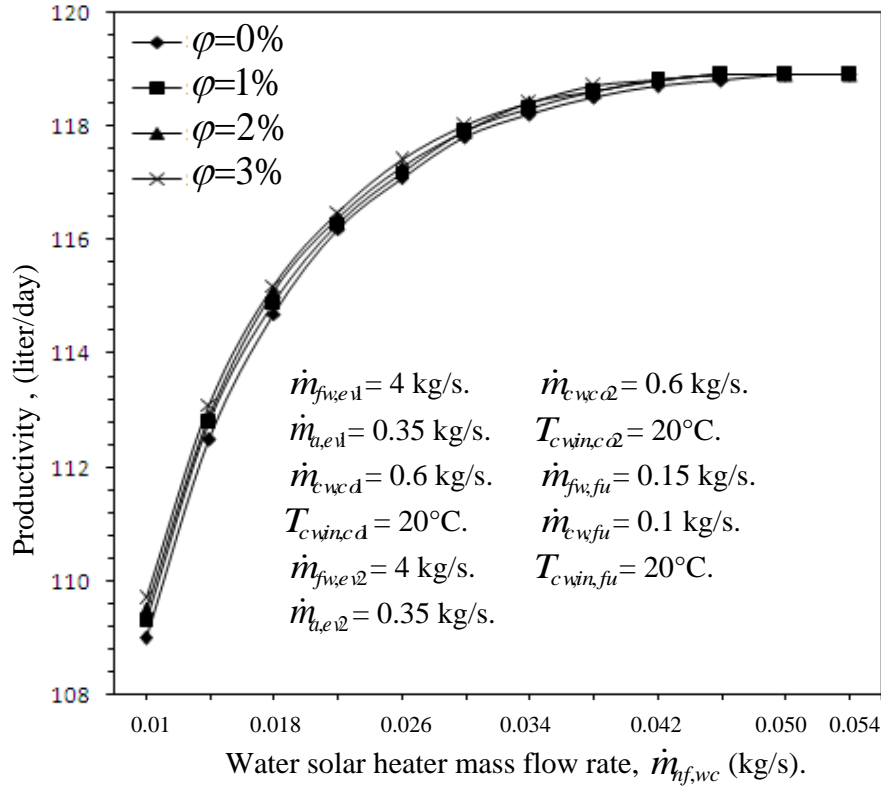

The figure contains the following legend and parameters:

$\varphi = 0\%$
$\varphi = 1\%$
$\varphi = 2\%$
$\varphi = 3\%$

$\dot{m}_{fw,ev1} = 4$ kg/s. $\dot{m}_{cw,c2} = 0.6$ kg/s.
$\dot{m}_{a,ev1} = 0.35$ kg/s. $T_{cwin,c2} = 20°C.$
$\dot{m}_{cw,cd} = 0.6$ kg/s. $\dot{m}_{fw,fu} = 0.15$ kg/s.
$T_{cwin,cd} = 20°C.$ $\dot{m}_{cw,fu} = 0.1$ kg/s.
$\dot{m}_{fw,ev2} = 4$ kg/s. $T_{cwin,fu} = 20°C.$
$\dot{m}_{a,ev2} = 0.35$ kg/s.

Axis: Productivity, (liter/day) vs Water solar heater mass flow rate, $\dot{m}_{nf,wc}$ (kg/s).

Figure 12.System productivity variations as a function of solar collector working fluid mass flow rate with different nano-particle volume fraction.

7.7. System performance

The system performance is investigated in this section. HDH-SSF cycles are traditionally heat driven cycles run by using low grade energy to heat the saline water and air. The efficiency of the cycle itself is measured by the gained output ratio (GOR) defined in Eqs. (43-44). The variation in GOR as a function of mass flow ratio $\left(\dot{m}_{fw,ev} / \dot{m}_a \right)$ of HDH unit is illustrated on

Figure (13). The GOR with mass flow ratio trend of HDH unit is non-linear. On the other hand, the GOR trend of SSF unit is approximately linear and constant at 1.048. So, GOR trend of both HDH stages is approximately the same for hybrid system. This due to heat recovery was occurred on mixing tank (MT) which rise the feed water temperature of humidifier (H1) and water closed loop for humidifier (H2). The gained output ratio (GOR) of the 1st stage and 2nd stage of HDH

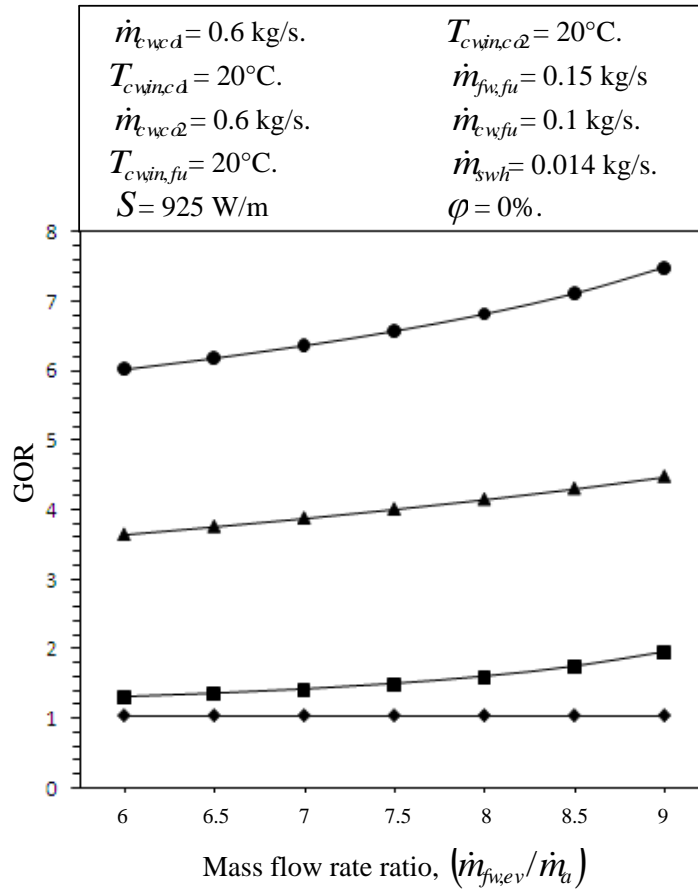unit reach 4.48 and 1.96 respectively at mass flow ratio 9.

Figure 13. Variations in GOR as a function of mass flow ratio $\left(\dot{m}_{fw,ev}/\dot{m}_a\right)$**of HDH units.**

Variations of solar water heater efficiency (η_{swh}) with different nano-particle volume fraction through day time are presented in Figure (14). It shows that the increasing of nano-particle volume fraction at constant working fluid mass flow rate the solar collector efficiency (η_{swh}) will increase. Explanation of these findings is the following: increasing the nano-particle volume fraction increases the thermal conductivity of the working fluid of solar collector that increase heat transfer coefficient inside solar water heater tubes, fluid outlet temperature and heat gained.
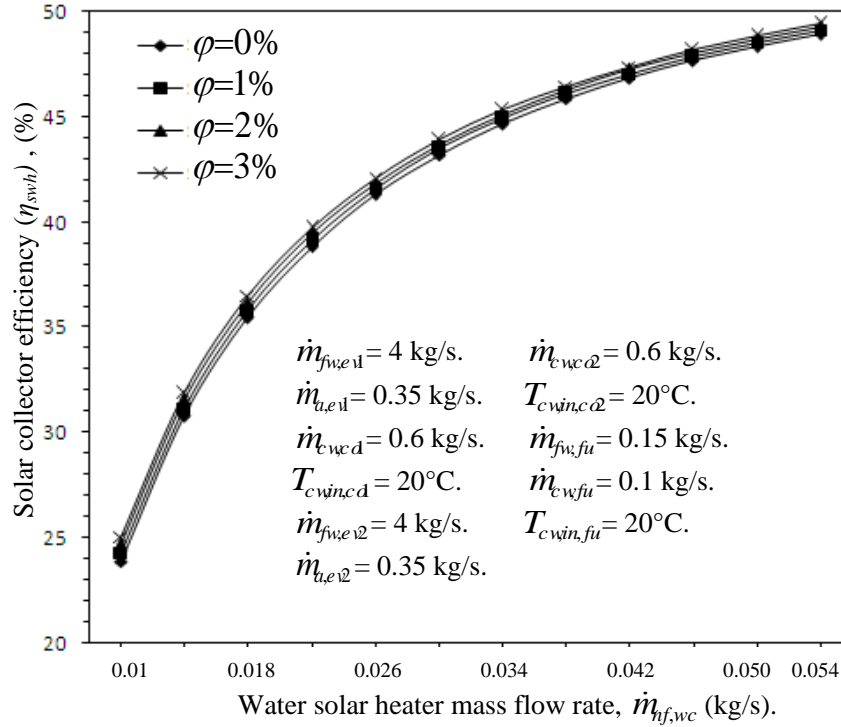
Figure 14. Solar collector efficiency (η_{swh}) variations as a function of solar collector working fluid mass flow rate with different nano-particle volume fraction at 12:00 AM.

Specific work consumption of the blower and pumps circulating the air and water based on m^3 of product water through the system was also calculated. It was found that for a blower and pumps efficiencies of 80%, the (MEH-SSF) was found to need 2.32 kWh/m³.

7.8. Cost analysis

Based on the previous analysis of the MEH-SSF plant, it can be seen that the final water production costs of two modes are calculated and compared to those of the conventional systems. That comparison is illustrated in Table (5). Although the solar powered small-scale systems tend to have higher costs per unit of fresh water output, the costs are still lower than the least cost spent for fresh water transportation by truck. In many remote areas, the reliability of delivered fuel is low. The fuel transportation cost over long distance and poor roads, is very high as declared by Ayoub and Alward [21]. Briefly, in isolated remote areas having no access to the electrical grid as well as suffering from a critical water supply shortage the cost and the profit will have a lower priority; hence the desalination with solar energy remains one of the most favorable choices for small capacity water desalting.

Table (5): Unit product cost of selected desalination units

Process	Capacity, m^3/day	Power	Cost, $/m^3	Reference
MEH-SSF	0.1125	Solar	6.43	Present system
HDH-SSF	0.096	Solar	12.53	[22]
HDH-SSF	0.088	Solar	13.08	[22]
HDH-SSF	0.077	Solar	17.71	[22]
HDH-SSF	0.089	Solar	14.23	[22]
Multi-effect still	10	Solar	28.8	[23]
MED	100	Solar	8.3-9.3	[24]
PV-RO	500	Solar	2.7	[25]
MD	0.5	Solar	18	[26]
MD	0.1	Solar	15	[27]
MD	17	Geothermal	13	[28]

7.9. Factors having an effect on water cost reduction

It can be observed from the mentioned cost analyses; there are many factors having an essential effect on the desalination cost. The adopted methods to reduce the cost of water production by desalination have been analyzed. These methods include the development of more efficient heat sources, the implementation of good manufacturing for the plant components and the use of correct maintenance programs.

7.9.1. Effect of plant life time

Figure (15) shows the water cost as a function of the plant lifetime, for the two modes of sea water desalination, the distilled water cost shows a significant decrease by increasing the plant lifetime. In fact, the expected life time for the different desalination plant components and their spent duration depend on the good manufacturing quality, the resistance of different components to corrosion and on the adopted maintenance program.
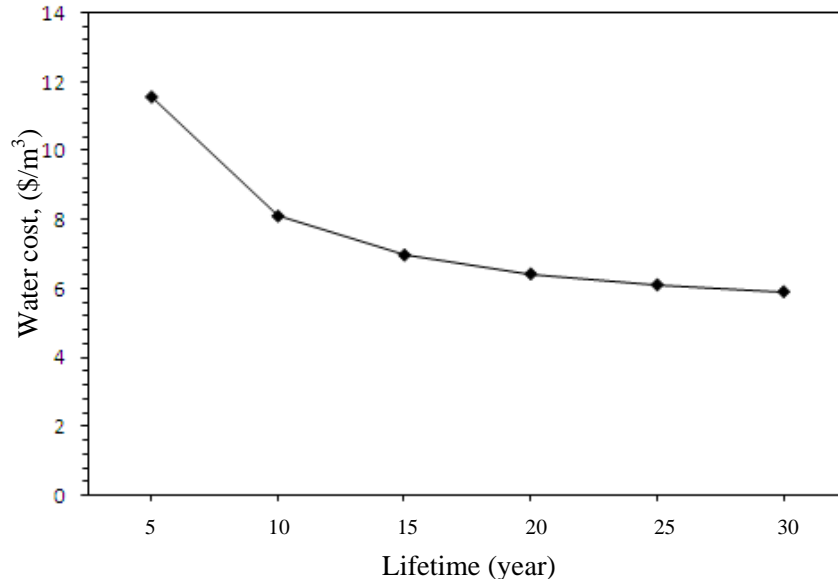
Figure 15. The effect of plant lifetime on the distilled water cost.

8   MODEL RESULTS VALIDATION

The main components of the program had been validated separately with another work. The solar water heater model had been validated by Matuska et al. [29]. While, the HDH and SSF models had been validated by Nafey et al. [3], Yamal and Solmus [22] and Nafey et al. [4] respectively. The present theoretical model had been compared and a good agreement with experimental data trend had been obtained. In addition, experimental replication of the proposed system is currently underway to validate model assumptions and predictions.

CONCLUSION

A theoretical investigation was carried out with the objective of studying a hybrid desalination system (MEH-SSF) consists of two stages of HDH unit and single stage flashing evaporation unit coupled with nano-fluid solar heater. Seven main parameters that have influence on the system productivity are feed water mass flow rate of SSF unit, feed water mass flow rate of HDH units, cooling water mass flow rate of SSF unit, cooling water mass flow rate of HDH units, air mass flow rate, inlet cooling water temperature and nano-particle volume fraction. The main conclusions are summarized:

1. A significant improvement on the HDH unit and SSF unit productivity can be achieved by hybridization and multi-effect humidification dehumidification, the daily water production up to 112.5 kg/day.
2. The MEH-SSF hybrid system productivity influenced by heat recovery when using mixing tank which gives GOR reaches 7.5.
3. The system performance of the unit was affected by the values of the inlet cooling water temperature and feed water mass flow rate.
4. Increasing the cooling water mass flow rate tends to increase the yield of fresh water productivity. The same trend is attained decreasing inlet cooling temperature.
5. The trend of air solar heater collecting area variation showed a pronounced increase in the fresh water productivity than that of the water solar heater collecting area variation.

6. The solar water heater efficiency is affected by the nano-particle volume fraction by increasing the fresh water production and decreasing cost.
7. The estimated cost of the potable water is about 6.43 US$/m^3.
8. Solar water heater efficiency is about 49.4%.
9. Specific work consumption is 2.32 kWh/m^3.

NOMENCLATURES

Latin Symbols

A	area, m^2
q	energy gain, W/m^2
C_p	specific heat, J/kgK
x	water salinity, ppm
g	gravitational constant, m^2/s
e	absorber plate to cover spacing and absorber plate to back plate spacing , m
h	heat transfer coefficient, W/m^2K
I	solar radiation rate, W/m^2
d	diameter, m
H	height, m
L	length, m
W	width, m
K	thermal conductivity, W/mK
F_R	collector heat removal factor, *dimensionless*
P	total system pressure, N/m^2
S	actual absorbing radiation solar energy, W/m^2
U	heat loss coefficient, W/m^2K
$\dot{m}$	Mass flow rate, kg/s
u	velocity, m/s
p	pressure, N/m^2
M	Mass fux (mass flow rate per unit area), $kg/s\ m^2$
a	area of heat transfer or mass transfer surface per unit of packing volume, m^2/m^3
k	mass transfer coefficient, m/s
T	Temperature, °C
$\overline{T}$	Average temperature, °C
F'	Collector efficiency factor, *dimensionless*
F	fin efficiency, *dimensionless*

Greek Symbols

α	solar absorptance of collector plate , *dimensionless*
β	collector tilt angle, *degree*
υ	kinetic viscosity, m^2/s
ω	humidity ratio, $kg_{water\ vapor}/kg_{dry\ air}$

ζ Packing void fraction, m^3/m^3

μ dynamic viscosity, $kg/m.s$

ρ density, kg/m^3

σ Stefan–Boltzmann constant $= 5.67\times10^{-8}\ W/m^2K^4$.

τ solar transmittance of glazing

δ thickness, m

θ V-groove angle, *degree*

Subscripts

1	object 1
2	object 2
a	air
w	fresh water
h	hydraulic
f	Fluid or flow
ac	air solar collector
wc	water solar collector
c	convection
t	top
am	ambient
o	out
r	radiation
in	in
p	heat-absorbing plate
lb	local base
b	bottom
bi	back insulation
e	edge
g1	First (top) layer of the glass cover
g2	Second (lower) layer of the glass cover
u	useful
row	row
m	mean
L	overall
s	saturation
H	heat transfer
M	mass transfer
v	vapor
V	V-groove
fg	difference between the saturated vapor and saturated liquid values of the same property
i	interface
cf	Condensate film
gc	glass cover
j	Node index

bo	bond
hot	Hot
cold	Cold
loss	loss
sw	sea water
iw	inside wall
cf	condensate film
cs	cross sectional
cw	Cooling water
ha	humid air
P	packing
0	property evaluated at 0 °C
cr	critical
sr	surface
wn	wind
T	total
d	dry
evap	evaporation
w-a	from water to air
dis	distillate
fin	fin
an	annulus
coil	coil
sh	shell
ev	humidifier
co	dehumidifier
calcul	calculated
guess	guessed
as	Air channel
ap	Aperture
fu	Flashing unit
bp	Brine pool
conv	Conventional
lm	Log mean
ss	Specific Surface
wet	Wet
wf	Water film
eq	equilibrium
su	Superheat
rv	removal
swh	Solar water heater

Superscripts

| e | estimated |

g　　　guessed

REFERENCES

A.E. Kabeel and Emad M. S El-Said, A hybrid solar desalination system of air humidification-dehumidification and water flashing evaporation: Part I. A numerical investigation, Desalination 320 (2013) 56-72.

A.E. Kabeel and Emad M. S El-Said, A hybrid solar desalination system of air humidification dehumidification and water flashing evaporation : A comparison among different configurations Desalination 330 (2013) 79-89.

A. Eslamimanesh, M.S. Hatamipour, Economical study of a small-scale direct contact humidification–dehumidification desalination plant. Desalination 250 (1) (2010) 203–207.

A.S. Nafey, H.E.S. Fath, S.O. El-Helaby, A.M. Soliman, Solar desalination using humidification dehumidification processes: Part II. An experimental investigation, Energy Conversion and Management 45 (2004) 1263–1277

A.S. Nafey, H.E.S. Fath, S.O. El-Helaby a, A. Soliman, "Solar desalination using humidification–dehumidification processes.Part II. An experimental investigation", Energy Conversion and Management, Vol.45, pp.1263–1277, 2004.

A.S. Nafey, M.A. Mohamad, S.O. El-Helaby, M.A. Sharaf, Theoretical and experimental study of a small unit for solar desalination using flashing process, Energy Conversion and Management 48 (2007) 528–538.

A.H. El-Shazly, A.A. Al-Zahrani, Y.A. Alhamed, S.A. Nosier, Productivity intensification of humidification–dehumidification desalination unit by using pulsed water flow regime, Desalination 293 (2012) 53–60.

Ayoub J, Alward R. Water requirements and remote arid areas: the need for small-scale desalination. Desalination 1996; 107(2):131–147.

Banat F, Jwaied N. Economic evaluation of desalination by small-scale autonomous solar-powered membrane distillation units. Desalination 2008; 220 (1):566–573.

Bouguecha S, Hamrouni B, Dhahbi M. Small scale desalination pilots powered by renewable energy sources: case studies. Desalination 2005; 183 (1):151–165.

C. Yamal and I. Solmus, A solar desalination system using humidification–dehumidification process: experimental study and comparison with the theoretical results, Desalination 220 (2008) 538–551.

El-Nashar AM. The economic feasibility of small solar MED seawater desalination plants for remote arid areas. Desalination 2001; 134 (4): 173–186.

Engineering Congress & Exposition, Denver, Colorado, USA.

Fiorenza G, Sharma VK, Braccio G. Techno economic evaluation of a solar powered water desalination plant. Energy Conservation Management 2003; 44 (14): 2217–2240

G. Prakash Narayan, Mostafa H. Sharqawy, H. John, V. Lienhard, Syed M. Zubair, Thermodynamic analysis of humidification dehumidification desalination cycles, Desalination and Water Treatment 16 (2010) 339–353**.**

H.P. Garg, R.S. Adhikari, K. Rakesh, Experimental design and computer simulation of multi-effect humidification-dehumidification solar distillation, Desalination 153 (2002) 81-86.

H.T. El-Dessouky, H.M. Ettouney, Fundamentals of Salt water Desalination", 1st Ed., ELSEVIER, 2002.

J. H. Lienhard, G. Prakash Narayan, Ronan K. McGovern, S. M. Zubair, Helium as a carrier gas in humidification dehumidification desalination systems, IMECE2011-62875, Proceedings of the ASME 2011 International Mechanical

J. Yogesh, Design and optimization of thermal systems, 2nd Ed., CRC Press.

L. G. Asirvatham , N. Vishal, S. K. Gangatharan, D. Mohanlal, Experimental Study on Forced Convective Heat Transfer with Low Volume Fraction of CuO Water Nanofluid, Energies 2 (2009) 97–119.

M. Saad, M. Ahmed, V. M. Morcos, Performance analysis of a vacuum desalination system. Proceedings of the ASME International Mechanical Engineering Congress & Exposition, Denver, Colorado, USA, 2011.

Rheinlaender J, Graeter F. Technologies for desalination of typically 10 m^3 of water per day. Desalination 2001; 139: 393–397.

S. Hou, H. Zhang, A hybrid solar desalination process of the multi-effect humidification-dehumidification and basin-type unit, Desalination 220 (2008) 552–557.

T. Yousefi, F. Veysi, E. Shojaeizadeh, S. Zinadini, An experimental investigation on the effect of Al2O3–H2O nano-fluid on the efficiency of flat-plate solar collectors, Renew. Energy 39 (2012) 293–298.

T. Matuska, V. Zmrhal, J. Metzger, Detailed modeling of solar flat – plate collectors with design tool KOLEKTOR 2.2, Eleventh International IBPSA Conference Glasgow, Scotland, July 27-30, 2009

W. Daungthongsuk, S. Wongwises, A critical review of convective heat transfer of nano-fluids, Renew. Sustain. Energy Rev. 11 (2007) 797–817**.**

Y.J. Dai, H.F. Zhang, 2000,"Experimental investigation of a solar desalination unit with humidification and dehumidification", Desalination, vol. 130, pp. 169–175.

Y. Junjie, Z. Dan, C. Daotong, W. Guifang, L. Luning, Experimental study on static/circulatory flash evaporation, International Journal of Heat and Mass Transfer 53 (2010) 5528–5535.

Y. Jaluria, Design and optimization of thermal systems. 2nd edition, CRC presses, 2007. p. 398.